The TiO_2/CuO heterostructure-based sensors for volatile organic compounds (VOCs) at room temperature (RT) measurements

Madina Sarsembina, Master student

Submitted in fulfilment of the requirements for the degree of Master of Chemical and Materials Engineering

School of Engineering and Digital Sciences
Department of Chemical and Materials Engineering

53 Kabanbay Batyr Avenue,
Astana, Kazakhstan, 010000

Supervisor: Almagul Mentbayeva
Co-supervisor: Amanzhol Turlybekuly

May 2023

DECLARATION

I hereby declare that this manuscript, entitled "The TiO_2/CuO heterostructure-based sensors for volatile organic compounds (VOCs) at room temperature (RT) measurements", is the result of my own work except for quotations and citations which have been duly acknowledged. I also declare that, to the best of my knowledge and belief, it has not been previously or concurrently submitted, in whole or in part, for any other degree or diploma at Nazarbayev University or any other national or international institution.

Name: Madina Sarsembina

Date: 03.05.2023

Abstract

For the purpose of evaluating air quality and keeping track of the release of dangerous substances into the environment, the detection of volatile organic compounds (VOCs) is crucial. For this purpose, a number of approaches have been developed, but the majority of them are either high-temperature operations or sophisticated equipment. Therefore, there is a lot of interest in the creation of inexpensive, portable sensors that are capable of detecting VOCs at room temperature. Metal oxide-based sensors have recently received much interest due to their sensitivity and selectivity towards different VOCs. TiO_2/CuO heterostructures have shown promise in this regard as materials for VOC sensing applications. TiO_2/CuO heterostructures have distinctive electrical characteristics and are readily fabricated using straightforward chemical processes. These heterostructures have been demonstrated to improve the sensitivity, selectivity, and response time of metal oxide-based sensors in order to improve their ability to detect a variety of VOCs.

In this study, using a scalable reactive magnetron sputtering technique at glancing angle deposition, we built an ultrasensitive gas-sensing device functioning at room temperature (RT). CuO/TiO_2 heterojunction nanointerfaces showed toluene, acetone, and ethanol gas sensitivity for approximately two times greater than TiO_2 mono-layer, and the device exhibits an excellent detection limit of 50 ppb at 25°C, short response, and recovery time (40 s and 52 s). The control over nanoarchitecture and similar size of the nanorod-like structure to the doubled Debye lengths (about 70–80 nm) are used to create the ultrasensitivity. The array of p-n heterojunction nanorods was exploited effectively and with minimal technical complexity in the applicable nanoarchitecture design, providing a flexible platform for various gas sensing devices. The statistical study of variances demonstrates that the data gathered is reliable and repeatable.

.

Acknowledgements

I'd like to sincerely thank Drs. Almagul Mentbayeva and Amanzhol Turlybekuly, who served as my thesis supervisors, for their direction, encouragement, and support throughout the entire project. Their tolerance, helpful critique, and insightful input have been crucial in determining the focus and calibre of my work.

I also want to express my gratitude to the Advanced sensors laboratory of National Laboratory Astana and Nazarbayev University's staff and faculty in the Chemical and Materials Engineering Department for their support and collaboration during my academic career. I am appreciative of the chances given to me for academic study, research, and development.

I want to express my gratitude to my family and friends for all they have done to support, inspire, and encourage me as I pursued my education. They have helped me overcome difficulties and barriers with their continuous support and confidence in my talents.

Finally, I'd want to thank everyone who kindly gave their time and effort to our study as research participants. The results of this study would not have been feasible without their involvement.

This study was supported by grants from Nazarbayev University (Grant No. 021220CRP0122 Development of highly sensitive MOS-based nano-film gas sensors) and the Science Committee of the Ministry of Education and Science of the Republic of Kazakhstan (Grant No. AP14872138 Innovative strategy to recognize the diabetic state of people: metal oxide nanorods as an ultrasensitive exhaled gas sensor).

Table of Contents

List of Abbreviations & Symbols

EDS (EDX)	Energy Dispersive X-ray Spectroscopy
FE - SEM	Field Emission Scanning Electron Microscopy
GLAD	Glancing Angle Deposition
GMS - 311	Gas Measurement System
MOS	Metal Oxide Semiconductor
ppb	Parts per billion
ppm	Parts per million
PS	Photoluminescence Spectroscopy
RT	Room Temperature
UPS	Ultraviolet Photoelectron Spectroscopy
Uv-vis	Ultra-visible Spectroscopy
VOC	Volatile Organic Compounds
XPS	X-ray Photoelectron Spectroscopy
XRD	X-ray Diffraction

List of Tables and Figures

Chapter 1 – Introduction

1.1 Aims and Objectives:

The work aims to develop an ultrasensitive gas sensor based on TiO_2/CuO heterostructures, which would increase the resistance. The higher modulation of resistance by the application of p-n heterostructures could be a good approach for enhancing the gas sensitivity at RT for VOCs.

The objective of the current research are:

- to give a comprehensive literature review on MOS gas sensors for VOCs
- development of TiO_2 and CuO thin films deposition parameters, to form nanorods like heterostructure
- research and optimization of the electrochemical and physical properties of the heterostuctured sensor.

1.2 Methodologies and Techniques:

Magnetron sputtering method, Field Emission Scanning Electron Microscopy (FE-SEM), Energy-Dispersive X-Ray Spectroscopy (EDS), X-Ray Diffraction (XRD), X-ray photoelectron Spectroscopy (XPS), UV-Vis Spectrophotometer (UV), Ultraviolet Photoelectron Spectroscopy (UPS), Gas measurement system (GMS-311), and current/voltage tests (I-V characteristics)

1.3 Literature Review:

The literature review comprises an introduction, general information about MOS gas sensors, features of p-type and n-type sensors' sensing principles, and problem specification of existing high-temperature operated MOS gas sensors.

1.4 Thesis Structure:

Five sections make up the master's thesis. The topic, an overview of the goals, and the thesis structure are all introduced in the first chapter. The literature review, which is covered in the second chapter, contains details on gas sensors, MOS gas sensors for VOCs, p-n heterostructured sensors, and the GLAD method. The third section provides an overview of the methods and supplies used in the research, including the magnetron sputtering technique, TCO substrate deposition, and experimental protocols. The experimental findings from XRD, FE-SEM, and XPS analysis for TiO_2/CuO heterojunction nanointerfaces are presented in the fourth part. The fifth section, which

concludes the study question comprehensively, outlines potential future directions and makes insightful suggestions for further investigation.

Chapter 2 – Literature Review

2.1 Introduction

Gas monitoring is a significant part of industrial processes, transportation, and residential activities. Flammable, hazardous gases, and organic vapors have all been detected using gas sensors. Exposure to VOCs can cause headaches, dizziness, and irritation of the eyes, nose, and throat, among other symptoms [1-3]. Gas monitoring devices for VOCs can be helpful in identifying and monitoring levels of these harmful compounds in the air. These devices can be used in a variety of settings, including homes, schools, and workplaces, to provide real-time information about air quality [2]. Even in healthcare industries for noninvasive disease detection and health monitoring using gas sensor biomarkers to analyze human breath. The study of human respiration is a promising avenue for accurately diagnosing a range of illnesses, as it contains a significant number of VOCs. This technique can even be employed to determine the concentration of acetone and glucose in the exhaled gas of individuals with diabetes. It is known that a person's breath contains acetone vapors that lead to the development of diabetes. Diabetes leads to millions of deaths every year, and it requires constant monitoring of blood glucose levels and constant treatment procedures, which are the most invasive and expensive [1-3]. The developed gas sensors, which work on the basis of biomarkers, help to detect severe diseases at the stage of their development. For the detection and treatment of diabetes, acetone sensors can be considered a unique tool, which allows the calculation of the amount of acetone contained. Also, for daily monitoring of blood glucose levels, it is necessary to develop a budget, portable and affordable acetone gas sensor. The use of MOS, which consist of metal oxides (ZnO, TiO_2, NiO, CuO, etc.), is a good solution for solving these problems [4].

2.2 Metal Oxide Semiconductors

Due to their exceptional gas sensitivity, metal-oxide semiconductors (MOS) are extensively used as gas sensing materials. These qualities allow them to have advantages over other gas-sensitive materials. The broad bandgap of these materials allows them to have a wide range of electrical properties. The material size has a significant impact on the properties of MOSs. The size of the MOS structures can affect various properties such as conductivity, mobility, and the electronic structure of the materials used. In particular, at the nanoscale, the properties of materials

can be significantly different from their bulk counterparts due to the emergence of new physical phenomena. This is commonly referred to as the “nano effect”, which can arise due to quantum confinement, surface effects, and changes in the atomic and electronic structure of the material. Therefore, it is important to consider the impact of the size and dimensionality of MOSs when designing and fabricating electronics devices [5].

Since metal oxide gas sensors have several advantages, such as low cost and ease of manufacture, they are used in health protection and the detection of explosive gases [6]. In order to detect VOCs, a MOS type of gas sensor is frequently utilized. It is crucial to develop MOS gas sensors that can identify VOCs for a number of reasons. VOCs are a particular class of air pollutants that can be harmful to both people's health and the environment. As mentioned previously regarding human health, exposure to high concentrations of VOCs can result in a variety of health issues, such as headaches, nausea, dizziness, and irritated eyes, noses, and throats. Long-term exposure to particular VOCs has also been connected to more severe health consequences, including cancer and damage to the liver and kidneys. VOCs have an effect on human health, but they also cause air pollution and climate change. Ground-level ozone can be detrimental to both people and plants when VOCs are released into the environment and react with other pollutants. Smog, which can decrease air quality and have an adverse effect on the ecosystem, is also a result of VOCs. Researchers and engineers can assist in locating and monitoring the sources of VOC emissions and taking action to limit them by creating MOS gas sensors that can detect VOCs. As shown in Table 1, several works have been done by detecting VOCs. This can serve to safeguard public health, enhance air quality, and lessen the environmental effects of VOCs [12-20].

Table 1. Sensing performance of MOS for VOCs

Sensor material	Concentration	Type of VOC	Operation temperature	Response, unit	Reference
$CuO/Cu_2O/Ag$	125 ppb	acetone	300^oC	8.04	[12]
Ru-doped ZnO	300 ppm	propane	300^oC	890	[13]

0.5% wt Ru-doped ZnO	50 ppm	ethanol	350°C	1.18	[14]
6% wt MoO_3-WO_3	100 ppm	acetone	375ºC	26.5	[15]
7.4% wt Sc-doped NiO	10 ppb	acetone	245°C	109.4	[16]
Al-NiO	100 ppm	ethanol	200°C	12	[17]
CuO	1000 ppm 1000 ppm 800 ppm	methanol ethanol acetone	220°C	5 7 8	[18]
NiO-Pt 0.7%	1 ppm 100 ppm	ethanol	200°C	2.17 20.85	[19]
SnO_2 nanolayer	100 ppm	n-buthanol	300ºC	17.3	[20]

Table 2

The working principle of MOS sensors is based on a change in the electrophysical properties of the sensitive layer of a semiconductor sample when the composition of the analyte gas medium changes. The polycrystalline film made of various types of metal oxides is used in a resistively superconductive gas sensor, the property of which is the electrical conductivity of the sensitive layer. The analogue voltage signal or resistance value is the rational output signal of a resistive sensor [6].

Depending on the type of detected impurity and the type of semiconductor conductivity, the resistance of the sensitive layer raises or decreases. When adsorption of acceptor particles (O_2) on the top of a semiconductor with n-type conductivity (in our case is ZnO), the resistance of the sensitive layer rises, and when adsorption of donor particles (H_2) decreases (donor signal); for semiconductors with p-type conductivity (NiO), the dependence is reversed [7]. A semiconductor sensor is a narrow insulating substrate (3×3 mm^2 or less) on which measuring electrodes and a

heater are located. The heater is necessary because the procedures occurring on the top of the semiconductor during the chemisorption of gases depend on temperature. The measuring electrodes are covered with a sensitive covering. Different sensor designs have been created; for instance, as illustrated in Figure 1, the detecting layer and sensor heater may be positioned on the same or opposite sides of the substrate [8]. It is preferable to use platinum or gold as the heater's material and measuring electrodes; other metals are also used to work with non-aggressive gases and the NiCr alloy.

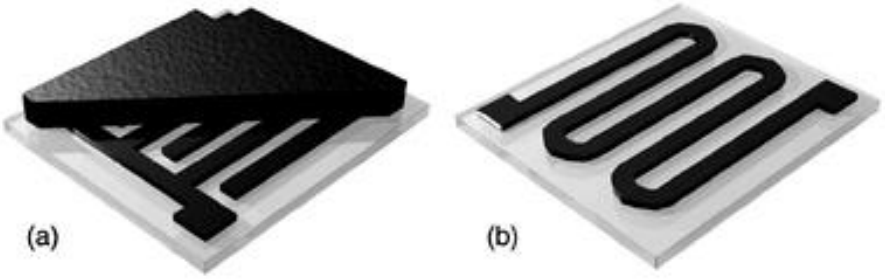

Figure 1. a) measuring electrode and b) heater of the sensor

The fundamental gas sensing mechanism of a resistive-based sensor is understood to be the modulation of the electrical resistance or conductance in a target gas environment. As oxygen molecules bind to the sensor's surface in air, an electron depletion layer (SDL) for n-type materials and a hole accumulation layer (HAL) for p-type materials will initially form. When an n-type MOS is exposed to an oxidizing source, its resistance increases, but reducing gates experience a decrease in resistance. The concept underpinning the n- and p-type MOS-based resistive gas sensors' gas detection procedure is schematically depicted in Figure 2 [9].

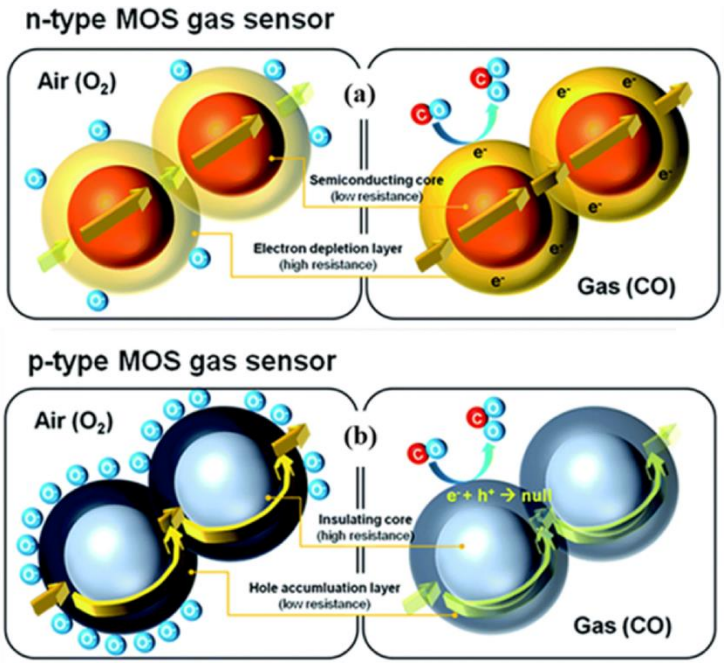

Figure 2. Basic sensing principle for n and p-type MOS gas sensors

An insulating substrate, interdigitated electrodes, and a heater that is positioned below the substrate to heat the sensor are the three main parts of chemiresistive-based sensors. Materials for the substrate are frequently chosen to be alumina or silicon oxide. Although the majority of MOS-based gas sensors operate at high temperatures between 100 and 450 °C, this heating process has a number of disadvantages, including decreased long-term stability due to the accumulation and coarsening of nanograins, increased fabrication costs because a heater is required, and high power consumption between 100 mW and 1 W. As a result, the issue of high power consumption restricts the integration of MOS-based gas sensors into several portable devices [9].

In breath sensing, MOS sensors are commonly utilized. Based on the chemiresistivity of MOS sensors, BIOSENSE Readout Health company has produced a high-resolution acetone meter [10]. The sensor composition and sensing conditions of the acetone meter are not defined on their official page or in related articles. Another device for acetone assessment is Keyto™, which is based on a nanostructured semiconducting metal oxide core that is selective to acetone. The chemical composition of the sensor was not declared. However, it was mentioned that measurement conducts at 400°C, see Figure 3 [11]. The elevated operating temperature of the sensor is a disadvantage due to high energy consumption. In a variety of sensing applications, surface characteristics including roughness, charge or surface potential, as well as the composition of Cu,

Ti or oxygen might affect the sensitivity and limit of detection. The surface area accessible for reaction can be impacted by surface roughness, changing sensitivity and limit of detection. Because more surface area is available for analyte interaction on a smoother surface, for instance, the limit of detection may be lower than it would be on a rougher surface. Particularly in electrochemical and biosensing applications, surface charge or potential can also influence sensitivity and limit of detection. This is such that the sensitivity and limit of detection can be affected by how analyte or biomolecule molecules bind to the sensor surface and how quickly they do so [11]. Similar to this, sensitivity and limit of detection can be affected by the composition of the Cu/Ti/O. Due to variations in their electrical and catalytic properties, the choice of metal oxide semiconductor employed in gas sensing applications, for instance, can considerably affect the sensitivity and limit of detection of distinct gases. In general, Cu/Ti/O surface characteristics and composition should be carefully examined during sensor design and optimization as they can significantly affect sensitivity and limit of detection in sensing applications.

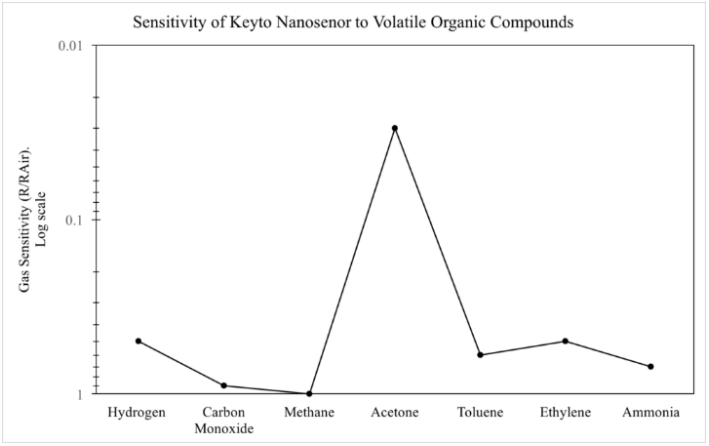

Figure 3. Sensitivity of the Keyto™ sensor to acetone and other volatile compounds at 400°C.

2.3 P-N heterostructures (HSs) via Glancing Angle Deposition (GLAD)

For usage in gas-sensing applications, MOS materials' nanostructures, including as nanowires, nanorods, and nanotubes, have recently attracted much attention due to their improved performance, high stability, low electron recombination rate, and high surface-to-volume ratio [10]. Conventional gas sensors typically have a single metal oxide layer, which limits their gas sensitivity and selectivity by detecting a change in bulk resistance in response to gas contact. The

construction of a p-n junction based on MOS is the best method for improving gas sensitivity and selectivity utilizing p-type and n-type electrodes. One of the most attractive types of p-n heterostructured MOS is the TiO_2-SnO_2 [22], TiO_2-CuO [21], ZnO-CuO [23], and CuO-SnO_2 [24].

With a broadband gap of roughly 3.0-3.2 eV, a high dielectric constant, excellent optical transparency, and exceptional chemical stability, titanium dioxide (TiO_2) often displays n-type MOS behavior. The cupric oxide (CuO) p-type semiconductor, on the other hand, has a narrow band gap closer to 1.2-1.5 eV and is used in a variety of applications, including gas detection and batteries [21]. As a result, it is wise to combine p-type and n-type semiconductors to create promising p-n heterojunctions. The p-n junction, where the electrons and holes are dimensionally separated, is made up of TiO_2 and CuO.

[25] investigated how to decorate gas sensors with the TiO_2-affected CuO. The study was shown good responses of 194-857% at 0.1-5ppm for H_2 gas. As shown in Figure 4, to check the sensitivity of sensors, a series of pulses of H_2 was given at 300C. The TiO_2-CuO had the same resistance before and immediately after each H_2 pulse, indicating that the response was reversible. The concentration of the given H_2 gas started from 0.1 to 5ppm.

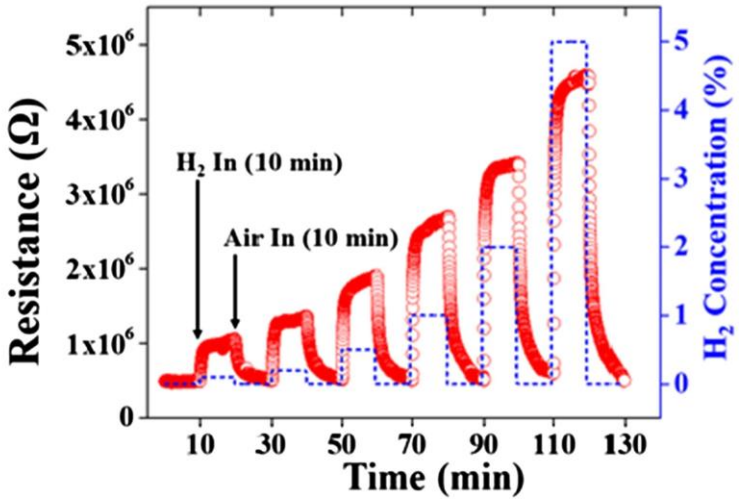

Figure 4. The responses of TiO_2 decorated CuO gas sensor exposed to-H_2 gas

[26] synthesized CuO-TiO_2 by using the chemical vapor deposition method. The performance of the synthesized gas sensor to H_2, O_3, and CH_3CH_2OH target gases was attractive, even in low temperatures. On the other hand, [27] compared CuO-TiO_2 with CuO-TiN gas sensing

materials. The last one shows a better response for CO_2 gas at 250°C (1000 ppm). With an increasing gas concentration, responses grow linearly.

A new transformed physical process called Glancing angle deposition (GLAD) is used to make complex and well-ordered nanostructures. Nanoplates, nanorods and nanocolumns are manufactured by this method [28]. Its main characteristic is the substrate surface's rotation and tilting at an angle greater than 80 degrees from the substrate surface's normal or less than 10 degrees from the direction of steam flow with respect to the normal of the substrate surface or less than 10 ° with respect to the direction of steam flow. As a result, isolated nanostructures are formed, obtained due to the "shadowing effect" by the physical process of self-assembly and surface diffusion experienced by vapor molecules. Through this method, such qualities of nanostructures as architecture, proportion, and density can be controlled using deposition parameters: working pressure, substrate temperature, displacement power, deposition angle, etc [28]. Several reports of the GLAD approach employing radio frequency (RF) and direct current (DC) magnetron sputtering to create WO_3, ZnO, and SnO_2 nanorods and other materials have been published [28–29]. A variable angle RF magnetron sputtering method was used to deposit carbon-doped and undoped WO_3 nanorods, as shown schematically in Fig.5 [28].

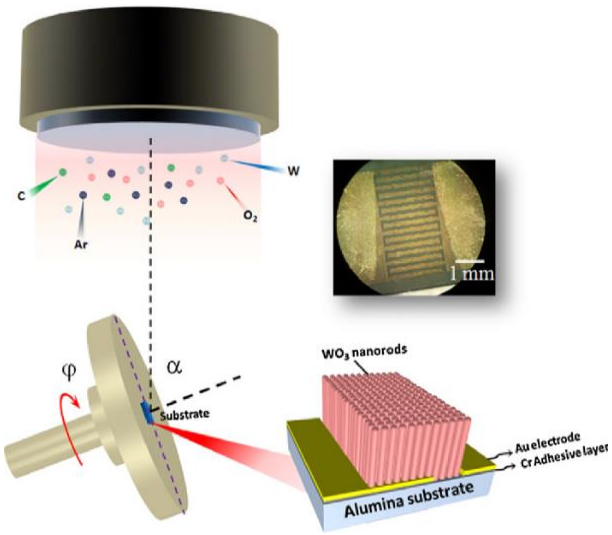

Figure 5. Carbon-doped WO_3 nanorods array fabricated by the Glancing-Angle RF Magnetron.

Chapter 3 – Materials and Methods

3.1 Material synthesis

TiO_2/CuO deposition. The first step in the preparation of gas sensors is the deposition of thin films via the magnetron sputtering method. First, 10 nm of Cr was deposited on the SiO_2 substrate for good adhesion; after 50nm of the bottom gold electrode will sputter on the surface of SiO_2. The primary synthetic pathway commences with the formation of p-n heterostructures. As shown in Fig.6, TiO_x was sputtered at a glancing angle of α=83° and a substrate rotation of 0.5 rpm via magnetron sputtering from a metallic Ti target in a reactive $Ar+O_2$ gas atmosphere. The deposition procedure continued until a film with a width of 120 nm was produced. The Cu_yO film is deposited under the identical circumstances, but the procedure is completed when the film is 30 nm wide. To create stable oxides with stable chemical compositions (CuO and TiO_2), thermal annealing was done in the presence of air. In order to optimize the annealing settings, the annealing process was carried out for 30 min at temperatures ranging from 450 to 650°C with 100°C increments. In order to prevent short circuits, a small separation from the bottom electrode was applied after the top gold electrode had been heated (Fig.6 step-2). The possibility of target gas absorption is greatly enhanced by the nanorod-like structure thanks to expanded sensing area compared to bulk materials and enlarged resistance alteration by a similar dimension of the single nanorod size to the Debye length. The third and final phase entails using a micro pattern to improve the sensing material's active surface area. The laser scribing technique was used to create tiny patterns (Fig. 6 step-3).

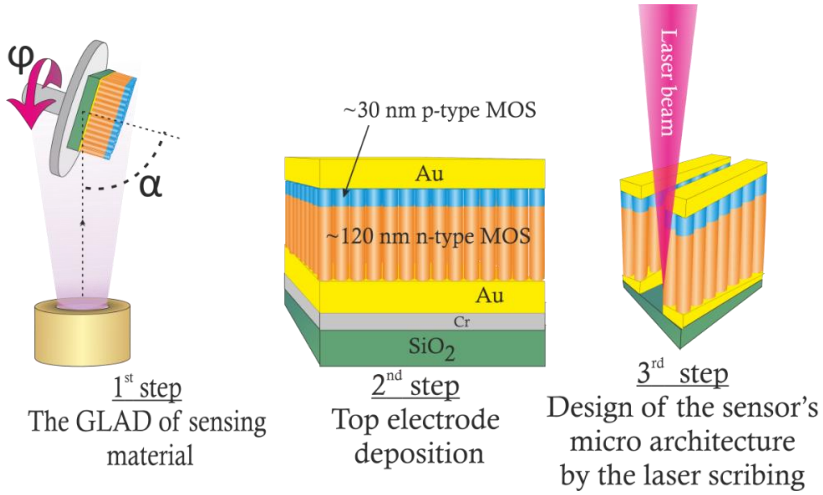

Figure 6. Schematic illustration of producing gas sensors

Magnetron sputtering. Magnetron sputtering is a method of obtaining coatings using cathode sputtering in a diode discharge plasma of crossed electric and magnetic fields. The main advantages of magnetron sputtering can be considered: high sputtering speed and adhesion, good cleanliness, ease of automation, and excellent uniformity on surfaces of large areas, as well as the ability to apply coatings on heat-sensitive substrates. Films obtained by magnetron sputtering have stoichiometry better representing the composition of the target material than the composition obtained by the method of thermal evaporation. The use of dual magnetron systems makes it possible to deposit several coatings in one technological cycle [30].

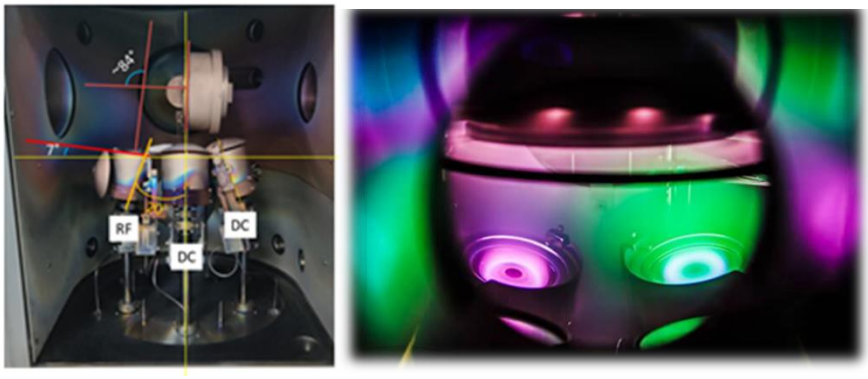

Figure 7. Magnetron sputtering system at C4-142, Core Facility

The deposition process was used to create a TiO_2/CuO film with a power input of 100W and an angle 83°**.** The oxygen concentration during the deposition process was 20%, and the burn-in time was 30 minutes, resulting in a thickness of 120 nm (TiO_2) with 5 hours deposition time. After the TiO_2 layer was deposited, a second deposition process was conducted to create a pure CuO layer. The power input was reduced to 30W, and the angle was set to 0°. The oxygen concentration was the same as before, 20%, and the burn-in time was only 10 minutes. This resulted in a thinner layer of only 30nm.

3.2 Materials Characterization and Sputtering Method

X-ray Diffraction (XRD). X-ray diffraction is an important tool for studying the crystallographic structure and phase composition of polycrystalline materials, including the possibility of studying violations of ideal crystallinity, that is, defects. The position of the reflexes in the diffraction pattern reflects the crystallographic symmetry (the size and shape of the unit cell),

while the intensity of the reflexes is related to the composition of the unit cell (the positions of the atoms). The shape of the diffraction lines indicates a deviation from ideal crystallinity [31]. Low-angle X-ray diffraction with a Cu Kα X-ray source was used in this experiment. Parameters for XRD analysis shown in Table 2.

Table 2. XRD parameters

2θ range	20 to 80°
Step size	0.04°
Wavelength	1.54Å
Speed duration time	3.0

Scanning Electron Microscopy (SEM). The Scanning Electron Microscope is a tool used to scan an object with a focussed electron beam and register a signal produced by the interaction of electrons with matter with a detector. This results in an enlarged image of the object. An electron source, an optical system for focusing and scanning electrons (an electronic column), a sample chamber, detectors for recording the signal, and a pumping system required to create a vacuum in the microscope are all shown in the scanning electron microscope's schematic picture [32].

Field emission scanning electron microscope (FESEM) (Germany's Zeiss CrossBeam-540) analysis of the sensors' nanostructure and morphology was performed using an energy dispersive (EDS) chemical composition analyzer from Oxford Instruments (UK). By using a Rigaku SmartLab diffractometer with a Cu Kα X-ray source, low-angle X-ray diffraction (XRD) was used to analyze the CuO/TiO_2 heterostructured nanorod's phase composition (Japan). Using the Evolution 300 UV-Vis Spectrophotometer (UV), absorbance spectra were measured to determine the optical band gap (Thermo Scientific, USA). Chemical bondings at the surface were identified using X-ray photoelectron Spectroscopy (XPS) (NEXSA, Thermo Scientific, USA). Chemical bondings at the surface were identified using X-ray photoelectron Spectroscopy (XPS) (NEXSA, Thermo Scientific, USA). On the same apparatus, Ultraviolet Photoelectron Spectroscopy (UPS) was used to calculate the molecular orbital energies in the valence region. Using the Hamamatsu Photonics spectrometer C9920-27102, Photoluminescence Spectroscopy (PL) was used to examine

relative changes in the electronic structure (Japan). The Keithley-2450 precision voltage and current source was used to record the electrical parameters (I-V characteristics) of the gas sensors.

3.3 Gas sensing measurements

The gas measurement system (GMS-311), which schematic is shown in Figure 8, was used to test the gas sensitivity and selectivity of the designed gas sensors. The gas sensing measurement system consists of a precision voltage and current source Keithley-2450, mass flow controllers (MFC-1,2), a humidity sensor, a 125 cm^3 test chamber, digital controller unit, cylinders (dry air and test gas) and PC. [33] states that Equation 1 was used to calculate the gas sensor sensitivity (S):

$$S_{sen} = \frac{|R_g - R_a|}{R_a} \times 100\%, \quad (1)$$

S_{sen} is the sensor's sensitivity, R_a an is its resistance to air, and R_g is its resistance when exposed to the target gas. The parameters were measured once every second. Every measurement was made at RT (around 25°C). By subjecting sensors to a target gas concentration of 5 ppm, selectivity tests were carried out. Gas was turned on for 1 minute, and it was turned off for 4 minutes using only air. The minimum concentration was chosen at 50 ppb, and the maximum concentration was set at 5 ppm because the goal of our work is to construct ultra-sensitive gas sensors. The time interval between the beginning of the target gas exposure and 90% response was used to calculate the gas sensor response time [33]. The recovery time was determined as the amount of time needed to relax before the target gas' background level was turned off [33,34]. In the experiment, each sensitivity and selectivity test was carried out three times. A two-factor analysis of variance (ANOVA) without a replication test for multiple comparisons was used for the statistical comparison [35]. At $p \leq 0.05$, statistical significance is regarded as dependable.

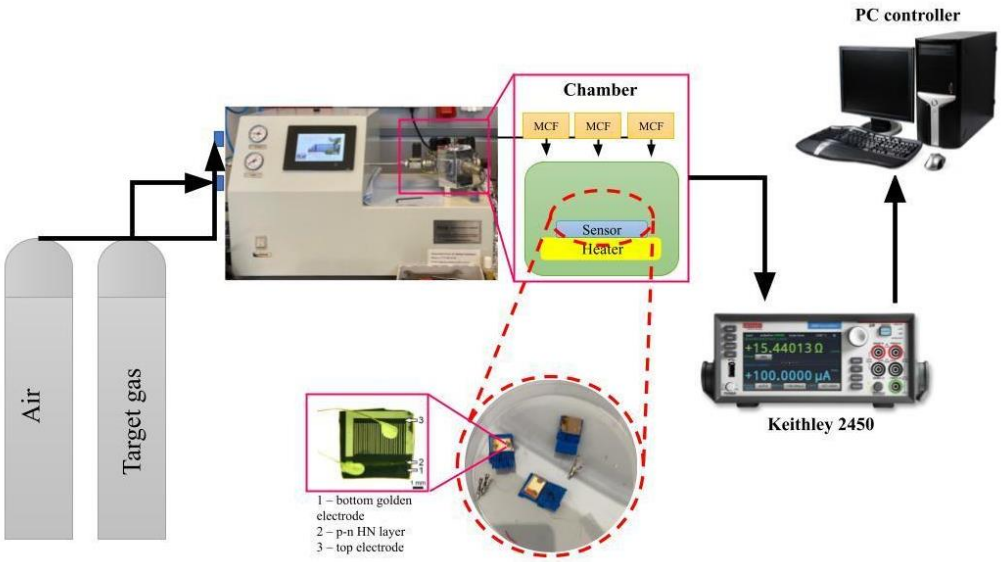

Figure 8. The schematic illustration of the gas sensing measurement system.

Chapter 4 – Results and Discussion

The experimental structure and operation of the gas sensor at RT are shown in Figure 9. As shown in Figure 9a, the p-n heterostructured nanorod has a number of benefits, including scalable size to Debye length, simple interaction with gas molecules, and a good adsorption/desorption ratio. A nanorod array is obtained using GLAD as part of the synthesis process, which is shown in Figure 9b, and is then subjected to thermal treatment, top golden electrode deposition, and laser scribing. The CuO layer has a thickness of 30 nm and is controlled by the idea of modifying nanostructured p-n interfaces. This method enables to immobilize charge carriers in all CuO layers, hence offering a scaled size to Debye length.

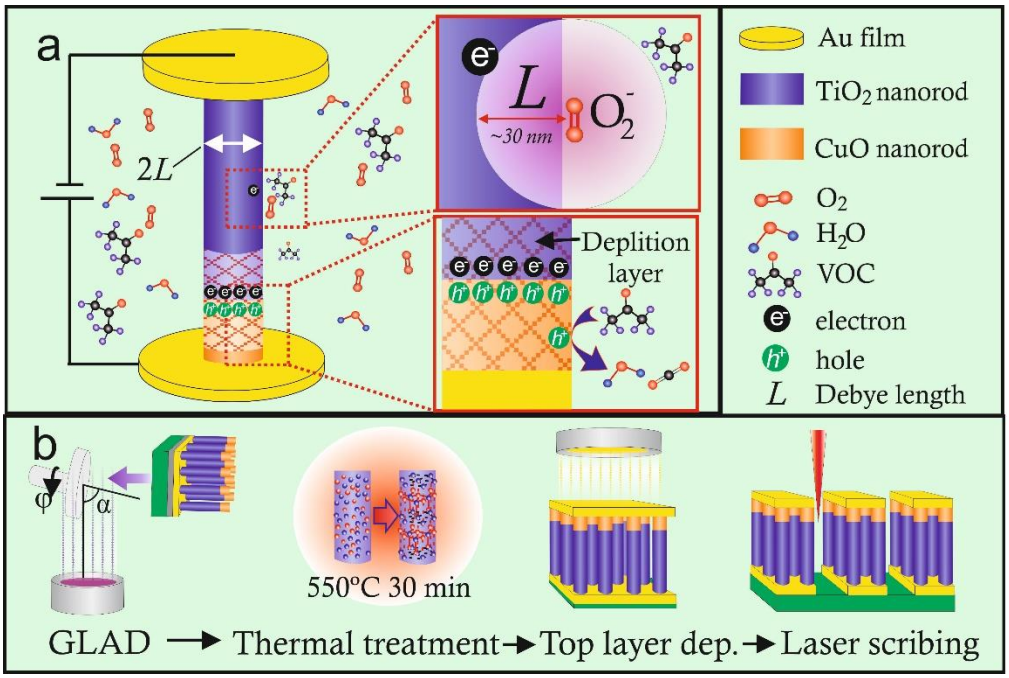

Figure 9. (a) The experimental design for the ultra-sensitive gas sensor at RT; (b) The plan for manufacturing sensors.

4.1 Materials Characterization

FESEM images of the top view and cross-section of samples prepared at different annealing temperatures was shown in Figure 10 (a-d). Different annealing temperatures show the gradient transformation process of the nanosized heterostructure. The optimal annealing temperature was found to be 550°C, which resulted in the transformation of the TiO_2 thin film to a nanorod-like structure with columnar separation, while the top Cu_yO layer agglomerated into isolated

nanoparticles as shown in Figure 10d. Increasing the temperature to 650°C led to structural decomposition and sublimation of the top layer, as shown in Figure A (Appendix A). The Cu_yO nanoparticles had a diameter of around 70-80 nm.

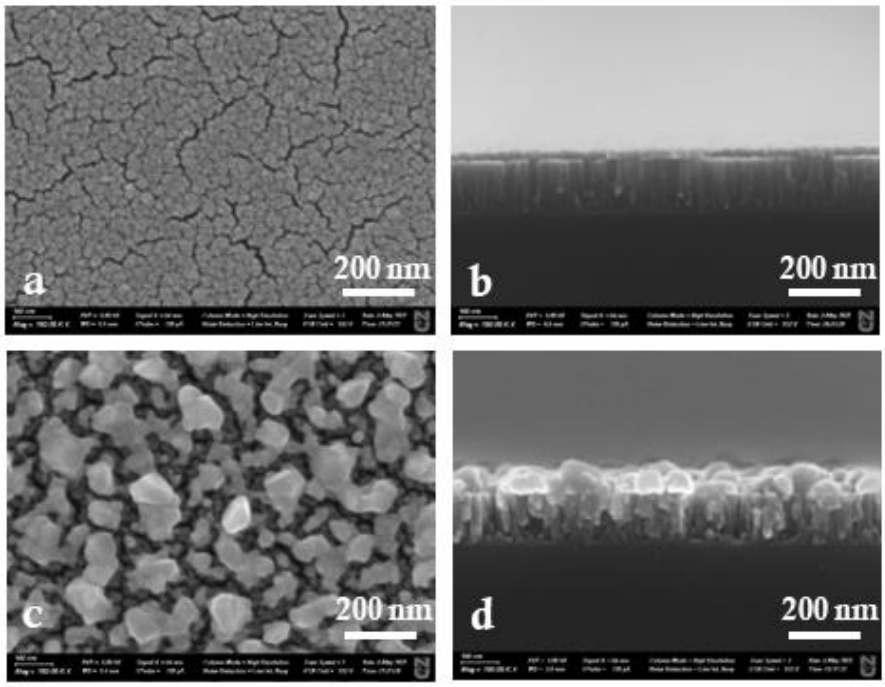

Figure 10. The FESEM images of the p-n heterostructures' morphologies before (a,b) and after heat treatment (c,d), top views (a,c), and cross-sections (b,d).

The EDX analysis (mapping) in Figure 11 (a-d) shows an uniform distribution of oxygen throughout all depths of the heterostructure, as seen in Figure 11b. The Ti (Fig.11d) and Cu (Fig.11c) were distributed mainly at the low layer (~120 nm) and the top layer (~30 nm), respectively, confirming the successful formation of the p-n heterostructure. The phase composition plays a critical role in MOS sensitivity, and there is a strong correlation between the crystallite size and gas sensing properties, as noted in previous studies [36,37]. Atomic percentage of Ti, Cu were found found 27.5 at wt%, 21 at wt%, as well as for oxygen 51.5 at wt%.

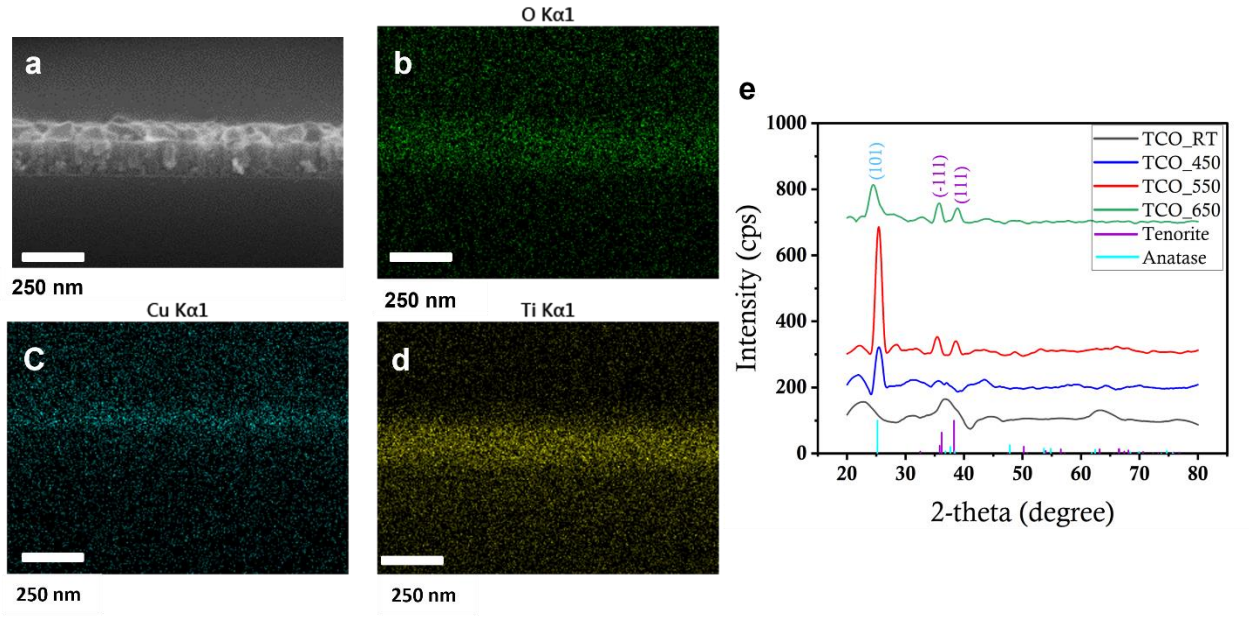

Figure 11. The EDX analysis of the p-n heterostructures: (a) image of observing area; (b) distribution of oxygen; (c) distribution of Cu; (d) distribution of Ti; (e) XRD patterns.

The samples were analyzed using XRD (ω=0.3), and the resulting patterns are shown in Figure 11e. It was discovered that the crystalline structure formation is heavily influenced by the annealing process. Specifically, at 450°C, the anatase (101) peak emerges, reaching its maximum intensity at 550°C, which may be due to an increase in crystallite size [38]. Tenorite peaks ((111) and its tween (-111)) with broadened peaks are present at higher temperatures of 550 and 650°C [39]. Consequently, it was determined that the best crystalline structure is formed at 550°C for 30 minutes of annealing, and further temperature increases resulted in amorphization.

The TiO_2 XPS pattern and the spin-orbit splitting value of Δ=5.7eV were highly associated [41] (Figure 12a). Due to the lack of a discernible difference between the Ti2p high-resolution spectra before and after thermal treatment, the XPS data supported the creation of TiO_2 during the reactive magnetron sputtering procedure. Cu 2p core level XPS spectra are shown in Figure 12b. After thermal treatment, the prominent $Cu2p_{1/2}$ and $Cu2p_{3/2}$ peaks shift to 953.9 eV (+1.5 eV) and up to 934.3 eV (+2.0 eV) with increasing the spin energy separation up to 19.6 eV, and their satellites intensity at 943 eV associate to $3d^{10}$ and $3d^9$ configuration [42] which is consistent with the oxidation state of 2+. The existence of distinct satellite peaks, a change in the major peak energies to 953.9 and 934.3 eV, and an increase in the FWHM of the Cu2p, which corresponds to

the higher oxidation state, are evidence that Cu_2O is converted to CuO during the thermal treatment [42].

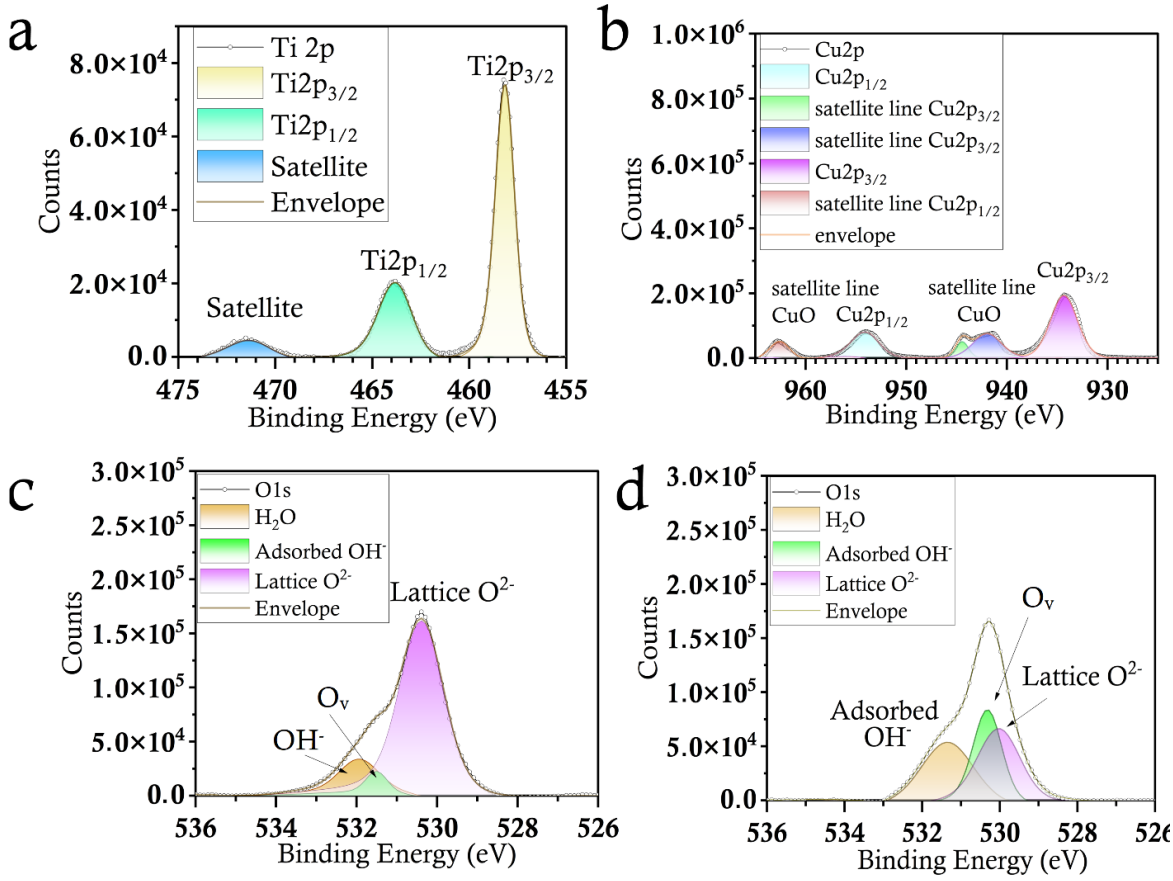

Figure 12. The XPS spectra of the p-n heterostructures after thermal treatment (550°C, 30min). (a) core level XPS spectra of Ti 2p; (b) core level XPS spectra of Cu 2p; (c, d) core level XPS spectra of O 1s before and after thermal treatment.

Figure 12c displays the high-resolution spectra of the O1s core level prior to thermal treatment. Lattice O^{2-} has the most intense peak at 530.4 eV (metal oxides). Both the peak at 531.5 eV and the peak at 532.0 eV have been classified as oxygen vacancies (O_v) and adsorbed aqueous species (OH^-), respectively [43]. The higher oxidation state of the system is determined by changes in the O1s XPS pattern following thermal treatment (see Figure 12d). Lattice O^{2-}specific main peak moves to a maximum of 529.4 eV. (-1 eV). The region of the peak of oxygen vacancies grows and the peak of oxygen vacancies changes up to 531.0 eV (+0.6 eV) (green-colored one, Figure 12d). Table 3 provides comprehensive details on the O1s core level XPS spectra. The number of oxygen vacancies (green peaks at 531.0–531.5 eV in Figure 12 c, d) increased by about 5 times compared

to the untreated sample, and the amount of adsorbed aqueous species increased by about 1.2 times, demonstrating the beneficial effects of thermal treatment on the formation of oxygen vacancies and adsorbed hydroxides (OH^-), which are crucial components of the gas sensing mechanism [44,45]. According to high-resolution O2s core level XPS spectra, the area shaded green under the Ov curve, the heat treatment converts Cu2O to CuO and greatly increases the concentration of adsorbed oxygen ions (Figure 12d). Also, until equilibrium, the thin CuO layer draws electrons from TiO_2 through the electric field that is already there, and at the same time, holes travel to TiO_2. The material's evident charge carrier deficient depletion layer is provided by the nanoscale architecture (150 nm in total width), which may account for the material's significantly higher gas sensor sensitivity.

Table 3. The data of O1s core level XPS spectra

	Name	Peak BE	Height, CPS	FWHM, eV	Area (P) CPS·eV
Before thermal treatment	Lattice O^{2-}	530.1	57 424	1.34	254 085
	Oxygen vacancies	531.5	20 509	0.65	15 467
	Adsorbed OH^-	532.0	31 341	1.2	44 210
After thermal treatment	Lattice O^{2-}	529.4	257 998	1.12	338 219
	Oxygen vacancies	531.0	52 523	1.42	87 364
	Adsorbed OH^-	532.2	15 274	2.93	52 425

Table 3

In order to determine the charge recombination rate in the CuO/TiO_2 heterostructure, Photoluminescence (PL) Spectroscopy was used. According to findings in the literature [46,47], the TiO_2 layer exhibits the highest PL emission intensity, as shown in Figure 13a. Figure 13a

demonstrates that the PL intensity of the p-n heterostructure is lower than that of CuO and TiO_2, which suggests that the electron-hole pair recombination is decaying [48,49]. A depletion layer that immobilizes charge transfer and so lengthens the lifespan of oxygen vacancies on TiO_2 and holes in CuO may be the cause of the reduced charge recombination [50,51]. The collected data is consistent with the findings of the XPS analysis, which revealed a rise in oxygen vacancies.

Using the use of UV-Vis absorbance spectra, and then constructing the Tauc plot, the optical band gap was determined. Figure 13b shows the CuO, TiO_2, and TCO heterostructure UV-Vis and Tauc plots. The passage of charge carriers from TiO_2's valence band to the conduction band is what causes the high absorption at 355 nm [48]. Meanwhile, adding a CuO layer modifies the absorption pattern a little. Decreasing absorbance that descends gradually suggests the presence of additional levels within the band gap [52], which was further supported by UPS results [52]. According to protocol [53], the optical band gap was determined using the Tauc plot for indirect absorption. Therefore, the band gap of the CuO/TiO_2 heterostructure was determined to be 2.96 eV and the band gap for the TiO_2 layers to be 3.49 eV. The increased energy levels within the TiO_2 band gap, which result in a reduced activation energy of the CuO/TiO_2 heterostructured sensor, may account for the declining value of the CuO/TiO_2 band gap [52]. The relative locations of the energy levels of the metal oxides in p-n heterojunctions CuO and TiO_2 determine the fundamental charge transfer mechanisms [54]. The UV-Vis and UPS results were compiled in order to experimentally determine the electronic structure and relative placements of energy levels. The UPS spectra were examined in order to determine the work function (φ), Fermi level (EF), and relative location of the valence band (EVB) in the energy diagram. The published work by Schlaf et al. [55] was used to determine the Fermi edge for each sample. Figure 13c shows the UPS (He I) spectra of TiO_2, CuO, and CuO/TiO_2 heterostructure. The work function was estimated as the difference between the cut-off level (16.11-17.11 eV, Figure 13c) and the UV light source energy (21.22 eV for He I) [56]. The distance between Fermi's level and the highest occupation state energy (EVF) was determined by applying the 2nd derivative computation to determine the valence band's relative position [54, 57] (Figure 13d dashed lines).

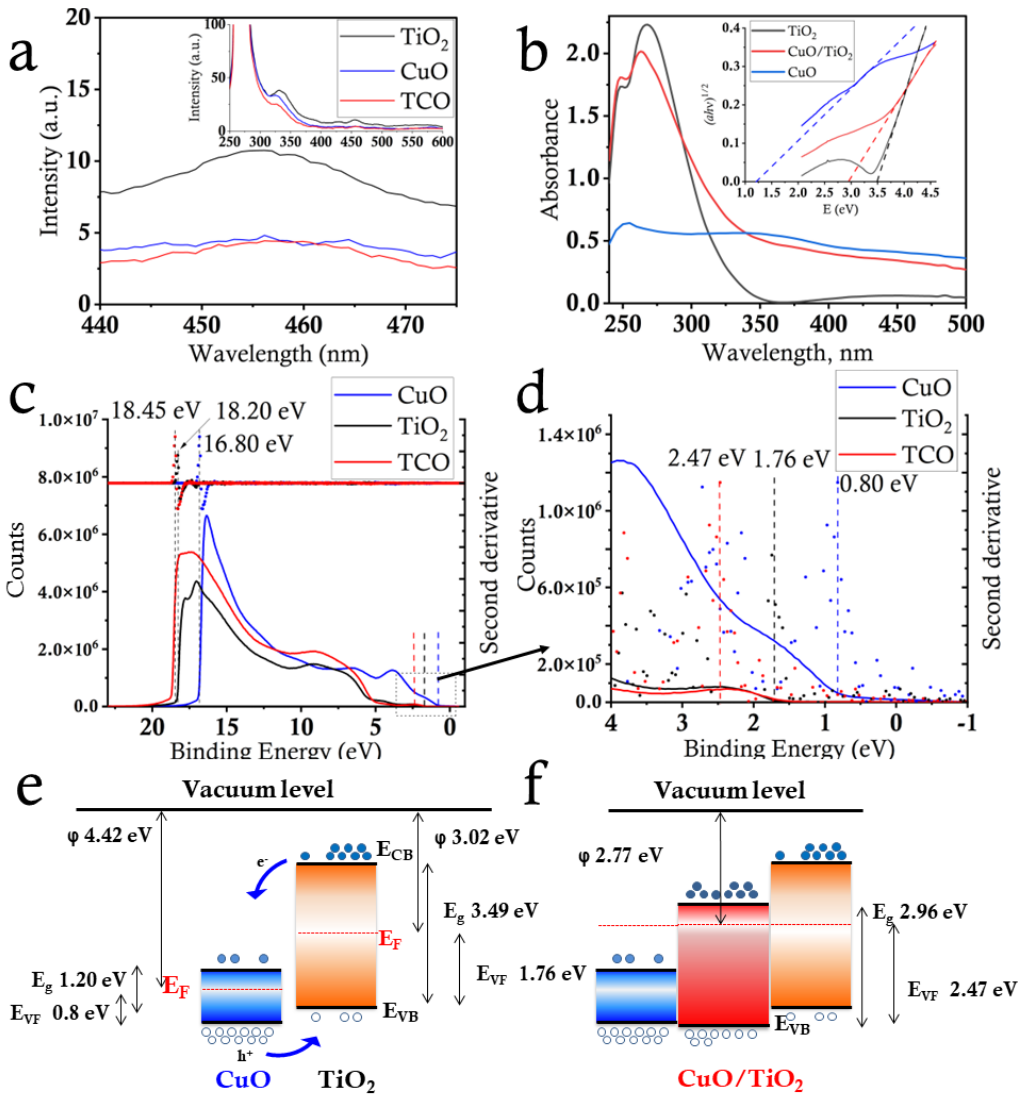

Figure 13. The band diagrams, UV-Vis spectra, and UPS of the heterostructures of CuO/TiO₂ and TiO₂/CuO. (a) PL spectra; (b) UV-Vis spectra; (c) the UPS spectra; and (d) the Tauc plot for the indirect band gap. The relative valence band location to EF is displayed

CuO has a work function value of -4.11 eV and a valence band position of -5.31 eV, respectively. As shown in Figure 13e, the TiO_2's work function was calculated to be -5.11 eV, and the valence band's location is - 8.42 eV. The built-in electric fields transport electrons to the CuO until the Fermi level reaches equilibrium [59] since the conduction band of TiO_2 is lower than that of CuO and the Fermi level is not aligned [58]. As a result, the charge carriers in the CuO/TiO_2 heterostructure immobilize, increasing sensitivity.

4.2 Sensor Characterization

At RT and 20% relative humidity, the nanorod-like TiO_2 and CuO/TiO_2 heterostructures were examined for their gas-sensing capabilities. In Figure B (Appendix B), the I-V characteristics are displayed. The sensor devices' ohmic voltage/current response was achieved with little perceptible resistance change. Figure 14 displays the outcomes of the sensitivity test. During the reproducibility test, the sensor device showed a reliable response when exposed to a 5 ppm concentration of acetone, ethanol, toluene and etc., gases (Figure 14a).

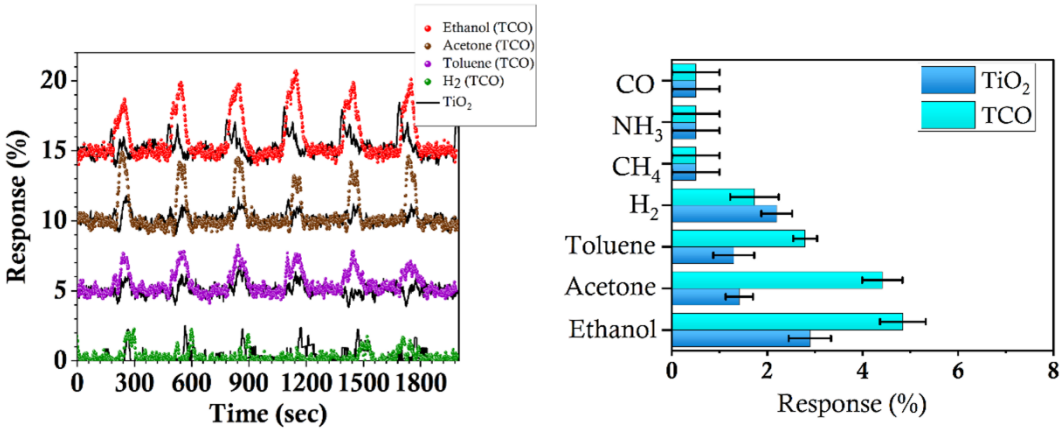

Figure 14. a) gas response of TiO_2 and p-n heterostructured nanorods toward 5 ppm VOCs at RT; b) selectivity of gas sensor prototype.

It can be shown that when exposed to the target gas, the sensor gadget produces precise and consistent responses. The application of the CuO layer improves the gas sensor's sensitivity, as shown in Figure 14a. According to PL and UPS data, it might be explained by the immobilization of charge transfer caused by the formation of a depletion layer, which prevents charge recombination and extends the lifespan of oxygen vacancies on TiO_2.

Three distinct samples were used for the gas sensing experiments, and the results were recorded and the average value determined. In gas sensing applications, the sensitivity of metal oxide sensors may decrease over time due to the aging of the sensing material, which can result in changes to the crystal structure and surface properties of the metal oxide. TiO_2/CuO gas sensors have been used for more than two months, and are still working. However, the response has become lower at the moment. The sensitivity was found to vary from sample to sample. Table B (Appendix B) displays the sensitivity of the sensor device's mean values. The results of the variance analysis revealed that the sample's influence is not statistically significant ($p=0.1494$), however, the sensitivity relies on the type of gas ($p = 5.0\times10^{-3} << 0.05$) (Table B).

Regarding quantitative and qualitative analysis, selectivity is among the most important properties of ultrasensitive gas sensors. The same conditions (5 ppm concentration and RT) were used for all selectivity experiments. Figure 14b displays the selectivity test results. Ethanol gas had the highest response (4.8%), which is near to response of acetone (4.4%). H_2 had the lowest reaction (1.7%), while sensors for gases including CH_4, CO, and NH_3 did not respond. It demonstrates the potential of newly created CuO/TiO_2 heterostructured nanorod-like devices as ethanol gas sensors.

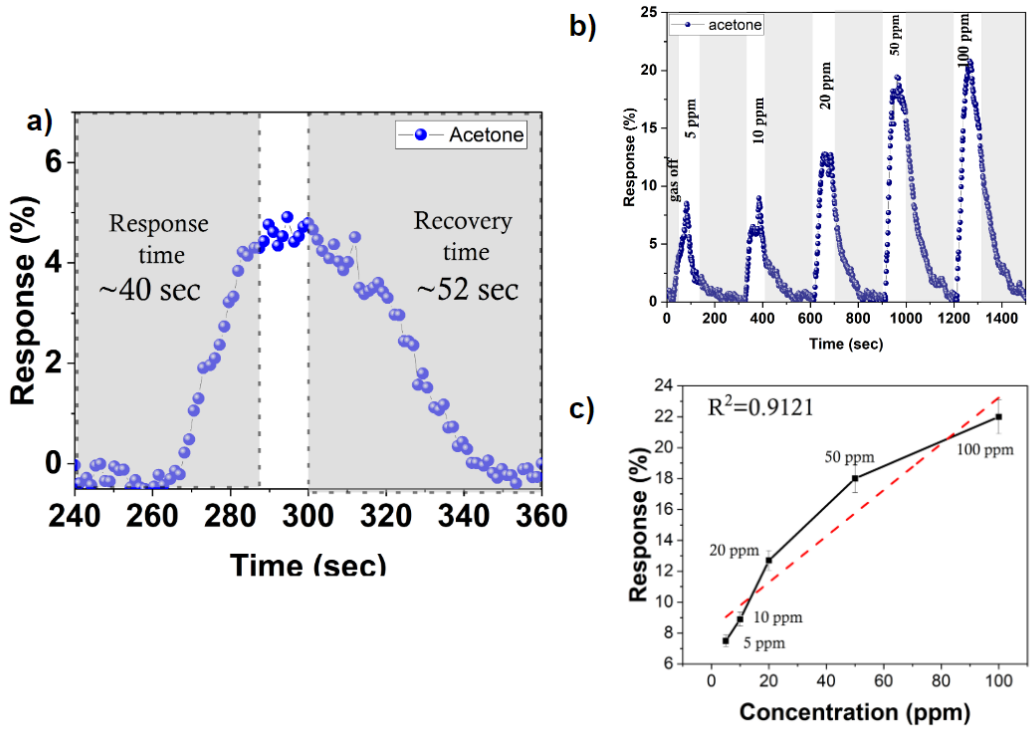

Figure 15. a) response and recovery time of acetone gas sensor; b) dynamic gas sensing test, the lowest detection is ~5ppm; c) calibration curve with uncertainties and the coefficient of determination R^2=0.9121

Figure 15a shows the results of the dynamic response test. Dynamic response analysis shows that the response time is only ~40s, but the recovery time is 52 s. The dynamic measurements of gas sensing at various concentrations of acetone gas exhibit strong linearity in the 5ppm to 100 ppm range, and the coefficient of determination has a respectable value (R^2=0.9121). Figure 15 (b,c). shows that the sensor device responded with 8.5% at a very low concentration of acetone (5 ppm) and with 22% at 100ppm.

Chapter 5 – Conclusion

CuO/TiO_2 heterostructured nanorod-like structure-based ultra-sensitive gas sensor device with a rapid response time has been developed. The scalable GLAD reactive magnetron sputtering technique was used for fabrication the gas sensor device. Thermal treatment was applied to increase the oxygen vacancies on the surface, which was proved by XPS analysis. The surface morphology, structure, and energy states of thin films were all thoroughly studied. It was shown, that CuO/TiO_2 heterostructure-based sensor has a high sensitivity at extremely low concentrations with a detection limit as low as 5 ppm and as high as 100 ppm. The sensor offers an impressive reaction time of ~40 s and recovery time of ~52 s, as well as a 22% response at 100 ppm (RT). Low response and recovery time are important characteristics for gas sensors because they determine how quickly the sensor can detect and respond to changes in gas concentrations. In applications such as air quality monitoring or industrial process control, it is important to quickly detect changes in gas concentrations to ensure the safety of the environment or the people working it. Regarding MOS gas sensors, a response of 22% at room temperature is considered high because it indicates that the sensor is sensitive enough to detect low concentrations of gas. According to the literature review, obtained results are promising for application in healthcare engineering. Large change in conductivity allows providing gas detection with high accuracy. To sum up, future studies on the development of gas sensors for the detection of acetone will concentrate on comprehending the theoretical underpinnings of sensor selectivity, refining the sensor structure by synthesis modification, and analyzing the impact of CuO layer thickness on sensor performance. The creation of gas sensors with high acetone selectivity and sensitivity will be made possible by addressing these research areas, and this will have a substantial impact on a variety of industrial and biomedical applications.

Bibliography/References

1. **Pargoletti, E., and G. Cappelletti**, "Breakthroughs in the Design of Novel Carbon-Based Metal Oxides Nanocomposites for VOCs Gas Sensing," Nanomaterials, 10(8), pp. 1485 (2020).
2. **Ciccioli, P.,** "VOCs and air pollution," in Bloemen, H.J.T., and Burn, J., eds., "Chemistry and Analysis of Volatile Organic Compounds in the Environment," Springer, Dordrecht, pp. 92-174 (1993).
3. **Schütze, A., *et al.,*** "Highly Sensitive and Selective VOC Sensor Systems Based on Semiconductor Gas Sensors: How to?," Environments, 4 (1), pp.20 (2017).
4. **Wongrat, E., *et al.,*** "Acetone gas sensors based on ZnO nanostructures decorated with Pt and Nb," Ceramics International, 43 (1), pp. S557–S566 (2017)
5. **Ji, H., *et al.,*** "Gas sensing mechanisms of metal oxide semiconductors: a focus review," Nanoscale, 11(47), pp. 22664–22684 (2019).
6. **Kwon, H., *et al.,*** "An array of metal oxides nanoscale hetero p-n junctions toward designable and highly-selective gas sensors," Sensors and Actuators B: Chemical, 255, pp. 1663–1670 (2018).
7. **Takada, T., *et al.,*** "Aqueous ozone detector using In_2O_3 thin-film semiconductor gas sensor," Sensors and Actuators B: Chemical, 25(1–3), pp. 548–551 (1995).
8. **Hansford, G. M., *et al.,*** "A low cost instrument based on a solid state sensor for balloon-borne atmospheric O_3 profile sounding," Journal of Environmental Monitoring, 7(2), pp.158 (2005).
9. **Majhi, S. M., *et al.,*** "Recent advances in energy-saving chemiresistive gas sensors: A review," Nano Energy, 79, pp.105369 (2021).
10. **Suntrup III, D. J., *et al.,*** "Characterization of a high-resolution breath acetone meter for ketosis monitoring," PeerJ, 8, pp.e9969 (2020).
11. **Keyto,** "The Science Behind Keyto, Part One – How The Keyto Breath Sensor Works," https://getkeyto.com/science-behind-keyto-how-the-breath-sensor-works, (2022).
12. **Choi, Y. M., *et al.,*** "Ultrasensitive Detection of VOCs Using a High-Resolution CuO/Cu_2O/Ag Nanopattern Sensor," Advanced Functional Materials, 29(9), pp.1808319 (2019).
13. **Gómez-Pozos, H., *et al.,* "**Chromium and Ruthenium-Doped Zinc Oxide Thin Films for Propane Sensing Applications," Sensors, 13(3), pp. 3432–3444 (2013).
14. **Xu, J., *et al.,*** "Studies on alcohol sensing mechanism of ZnO based gas sensors," Sensors and Actuators B: Chemical, 132(1), pp. 334–339 (2008).
15. **Zhang, J., *et al*.**, "Porous bimetallic Mo-W oxide nanofibers fabricated by electrospinning with enhanced acetone sensing performances," Journal of Alloys and Compounds, 779, 531–542 (2019).
16. **Tong, B., *et al.,*** "Sc-doped NiO nanoflowers sensor with rich oxygen vacancy defects for enhancing VOCs sensing performances," Journal of Alloys and Compounds, 851, pp.155760 (2021).
17. **Wang, C., *et al.,*** "Design of Superior Ethanol Gas Sensor Based on Al-Doped NiO Nanorod-Flowers," ACS Sensors, 1(2), pp.131–136 (2016).

18. **Yang, C., *et al.,*** "Facile microwave-assisted hydrothermal synthesis of varied-shaped CuO nanoparticles and their gas sensing properties," Sensors and Actuators B: Chemical, 185, pp. 159–165 (2013).
19. **Fu, J., *et al.,*** "Enhanced Gas Sensing Performance of Electrospun Pt-Functionalized NiO Nanotubes with Chemical and Electronic Sensitization," ACS Applied Materials & Interfaces, 5(15), pp. 7410–7416 (2013).
20. **Sun, F., *et al.,*** "Direct Growth of Mono and Multilayer Nanostructured Porous Films on Curved Surfaces and Their Application as Gas Sensors," Advanced Materials, 17(23), pp. 2872–2877 (2005).
21. **Maziarz, W.,** "TiO_2/SnO_2 and TiO_2/CuO thin film nano-heterostructures as gas sensors," Applied Surface Science, 480, pp. 361–370 (2019).
22. **Marzec, A., *et al.,*** "Preparation of nanocrystalline heterostructures TiO_2-SnO_2 by modified sol-gel method," Mechanik, 5(6), pp. 506–507 (2016).
23. **Poloju, M., *et al.,*** "Improved gas sensing performance of Al doped ZnO/CuO nanocomposite based ammonia gas sensor," Materials Science and Engineering: B, 227, pp. 61–67 (2018).
24. **Shao, F., *et al.,*** "Heterostructured p-CuO (nanoparticle)/n-SnO_2 (nanowire) devices for selective H_2S detection," Sensors and Actuators B: Chemical, 181, pp. 130–135 (2013).
25. **Park, S., *et al.,*** "Synthesis and Hydrogen Gas Sensing Properties of TiO_2 -decorated CuO Nanorods," Bulletin of the Korean Chemical Society, 36(10), pp. 2458–2463 (2015).
26. **Barreca, D., *et al.,*** "Novel Synthesis and Gas Sensing Performances of CuO–TiO_2 Nanocomposites Functionalized with Au Nanoparticles," The Journal of Physical Chemistry C, 115(21), pp.10510–10517 (2011).
27. **Lim, C.H., *et al.,*** "gas-sensing properties of CuO-TiN and CuO-TiO_2 prepared via an oxidizing process of a Cu-TiN composite synthesized by a mechanically induced gas-solid reaction," Metals and Materials International, 20(2), pp.323–328 (2014).
28. **Wongchoosuk, C., *et al.,*** "Carbon doped tungsten oxide nanorods NO_2 sensor prepared by glancing angle RF sputtering," Sensors and Actuators B: Chemical, 181, pp.388–394 (2013).
29. **Lin, S.S., *et al.,*** "The properties of Ti-doped ZnO films deposited by simultaneous RF and DC magnetron sputtering," Surface and Coatings Technology, 191(2–3), pp. 286–292 (2005).
30. **Swann, S.,** "Magnetron sputtering," Physics In Technology, 19(2), pp. 67-75 (1988).
31. **Drickamer, H., *et al.,*** "X-Ray Diffraction Studies of the Lattice Parameters of Solids under Very High Pressure," Solid State Physics, pp.135-228 (1987).
32. "Scanning electron microscope | Definition, Images, Uses, Advantages, & Facts," Encyclopedia Britannica, (2022).
33. **Soltabayev, B., *et al.,*** "Quick NO Gas Sensing by Ti-Doped Flower–Rod-like ZnO Structures Synthesized by the SILAR Method," ACS Applied Materials & Interfaces, 14(36), pp. 41555–41570 (2022).
34. **Yergaliuly, G., *et al.,*** "Effect of thickness and reaction media on properties of ZnO thin films by SILAR," Scientific Reports, 12(1), 851 (2022).
35. **Heiberger, R. M., and B. Holland**, "Statistical Analysis and Data Display," Springer, New York (2015).

36. **Iwamoto, M., *et al.,*** "Study of metal oxide catalysts by temperature programmed desorption. 4. Oxygen adsorption on various metal oxides," The Journal of Physical Chemistry, 82(24), pp. 2564–2570 (1978).
37. **Yamazoe, N.,** "Toward innovations of gas sensor technology," Sensors and Actuators B: Chemical, 108(1–2), pp. 2–14 (2005).
38. **Shukla, G., and S. Angappane,** "Dimensional constraints favour high temperature anatase phase stability in TiO_2 nanorods," Applied Surface Science, 577, pp. 151874 (2022).
39. **Ethiraj, A. S., and D. Kang,** "Synthesis and characterization of CuO nanowires by a simple wet chemical method," Nanoscale Research Letters, 7(1), pp. 70 (2012).
40. **Bharti, B., *et al.,*** "Formation of oxygen vacancies and Ti^{3+} state in TiO_2 thin film and enhanced optical properties by air plasma treatment," Scientific Reports, 6(1), pp. 32355 (2016).
41. **Zhang, E., *et al.,*** "Novel synthesis of S-doped anatase TiO_2 via hydrothermal reaction of Cu–Ti amorphous alloy," Applied Physics A, 126(8), pp. 606 (2020).
42. **Kulkarni, P., *et al.,*** "Photoelectron spectroscopic studies on a silicon interface with $Bi_2Sr_2CaCu_2BO_{8+\delta}$ high T_c superconductor," Journal of Applied Physics, 67(7), pp. 3438–3442 (1990).
43. **Saha, J. K., *et al.,*** "Significant improvement of spray pyrolyzed ZnO thin film by precursor optimization for high mobility thin film transistors," Scientific Reports, 10(1), pp. 8999 (2020).
44. **Meng, D., *et al.,*** "Rational design of CuO/In_2O_3 heterostructures with flower-like structures for low temperature detection of formaldehyde," Journal of Alloys and Compounds, 896, pp. 162959 (2022).
45. **Zhang, Y., and J. Mu,** "Controllable synthesis of flower- and rod-like ZnO nanostructures by simply tuning the ratio of sodium hydroxide to zinc acetate," Nanotechnology, 18(7), pp. 075606 (2007).
46. **Kong, J., *et al.,*** "Homeostasis in $Cu_xO/SrTiO_3$ hybrid allows highly active and stable visible light photocatalytic performance," Chemical Communications, 53(91), pp. 12329–12332 (2017).
47. **Shi, Q., *et al.,*** "CuO/TiO_2 heterojunction composites: an efficient photocatalyst for selective oxidation of methanol to methyl formate," Journal of Materials Chemistry A, 7(5), pp. 2253–2260 (2019).
48. **Zhang, S., *et al.,*** "CuO Nanoparticle-Decorated TiO_2 -Nanotube Heterojunctions for Direct Synthesis of Methyl Formate *via* Photo-Oxidation of Methanol," ACS Omega, 5(26), pp. 15942–15948 (2020).
49. **Zhu, X., *et al.,*** "One-step hydrothermal synthesis and characterization of Cu-doped TiO2 nanoparticles/nanobucks/nanorods with enhanced photocatalytic performance under simulated solar light," Journal of Materials Science: Materials in Electronics, 30(14), pp. 13826–13834 (2019).
50. **Sun, M., *et al.,*** "Photo-driven Oxygen Vacancies Extends Charge Carrier Lifetime for Efficient Solar Water Splitting," Angewandte Chemie International Edition, 60(32), pp. 17601–17607 (2021).
51. **Zhang, L., *et al.,*** "Effects of oxygen vacancies on the photoexcited carrier lifetime in rutile TiO_2," Physical Chemistry Chemical Physics, 24(8), pp. 4743–4750 (2022).

52. **Carlson, B., *et al.,*** "Valence Band Alignment at Cadmium Selenide Quantum Dot and Zinc Oxide $(10\bar{1}0)$ Interfaces," The Journal of Physical Chemistry C, 112(22), pp. 8419–8423 (2008).
53. **Makuła, P., *et al.,*** "How To Correctly Determine the Band Gap Energy of Modified Semiconductor Photocatalysts Based on UV–Vis Spectra," The Journal of Physical Chemistry Letters, 9(23), pp. 6814–681 (2018).
54. **Maheu, C., *et al.,*** "UPS and UV spectroscopies combined to position the energy levels of TiO_2 anatase and rutile nanopowders," Physical Chemistry Chemical Physics, 20(40), pp. 25629–25637 (2018).
55. **Schlaf, R., *et al.,*** "Determination of interface dipole and band bending at the Ag/tris (8-hydroxyquinolinato) gallium organic Schottky contact by ultraviolet photoemission spectroscopy," Surface Science, 450(1–2), pp. 142–152 (2000).
56. **Shao, G.,** "Work Function and Electron Affinity of Semiconductors: Doping Effect and Complication due to Fermi Level Pinning," Energy & Environmental Materials, 4(3), pp. 273–276 (2021).
57. **Watts, J. F., and J. Wolstenholme,** "An Introduction to Surface Analysis by XPS and AES," John Wiley & Sons, Ltd (2003).
58. **Moniz, S. J. A., and J. Tang,** "Charge Transfer and Photocatalytic Activity in CuO/TiO_2 Nanoparticle Heterojunctions Synthesised through a Rapid, One-Pot, Microwave Solvothermal Route," ChemCatChem, 7(11), pp. 1659–1667 (2015).
59. **Lei, M., *et al.*,** "Photocatalytic reductive degradation of polybrominated diphenyl ethers on CuO/TiO_2 nanocomposites: A mechanism based on the switching of photocatalytic reduction potential being controlled by the valence state of copper," Applied Catalysis B: Environmental, 182, pp. 414–423 (2016).

Appendix – A

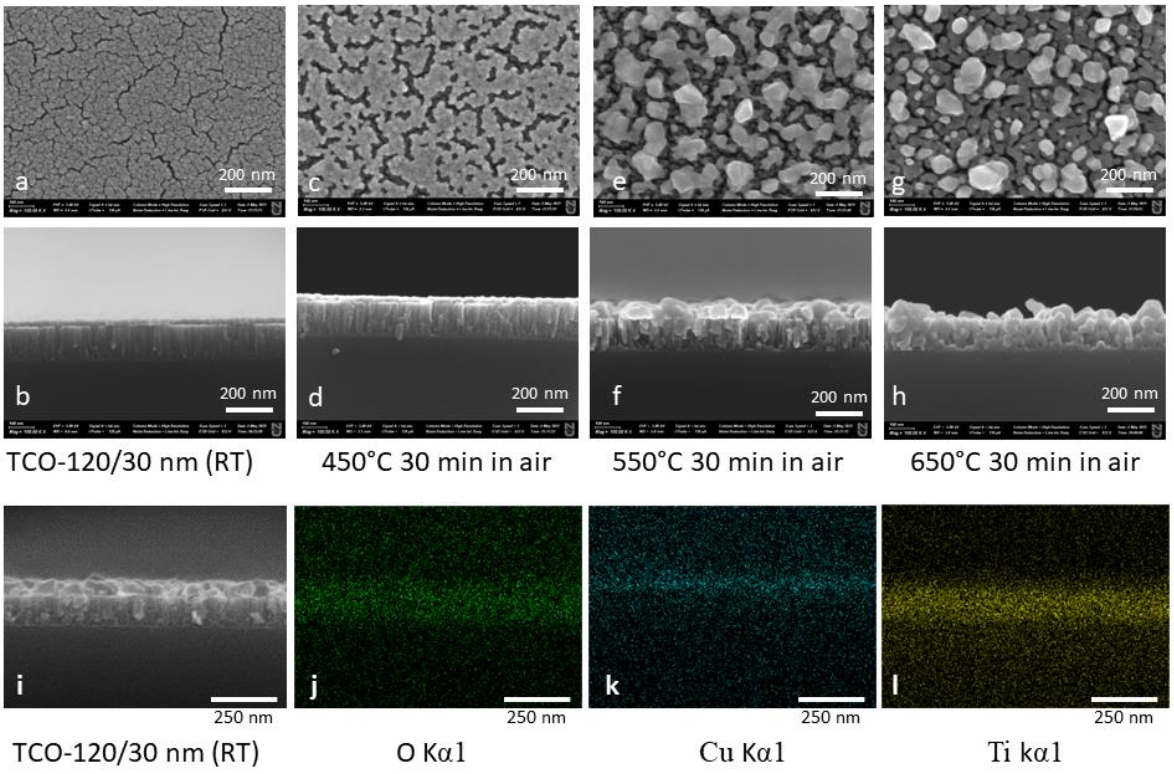

Figure A. The FESEM images of the p-n heterostructures' morphologies and cross-section images after different heat treatment parameters (a-h). The EDX analysis of the p-n heterostructures: i) image of observing area; j) distribution of oxygen k) distribution of Cu; l) distribution of Ti;

Appendix – B

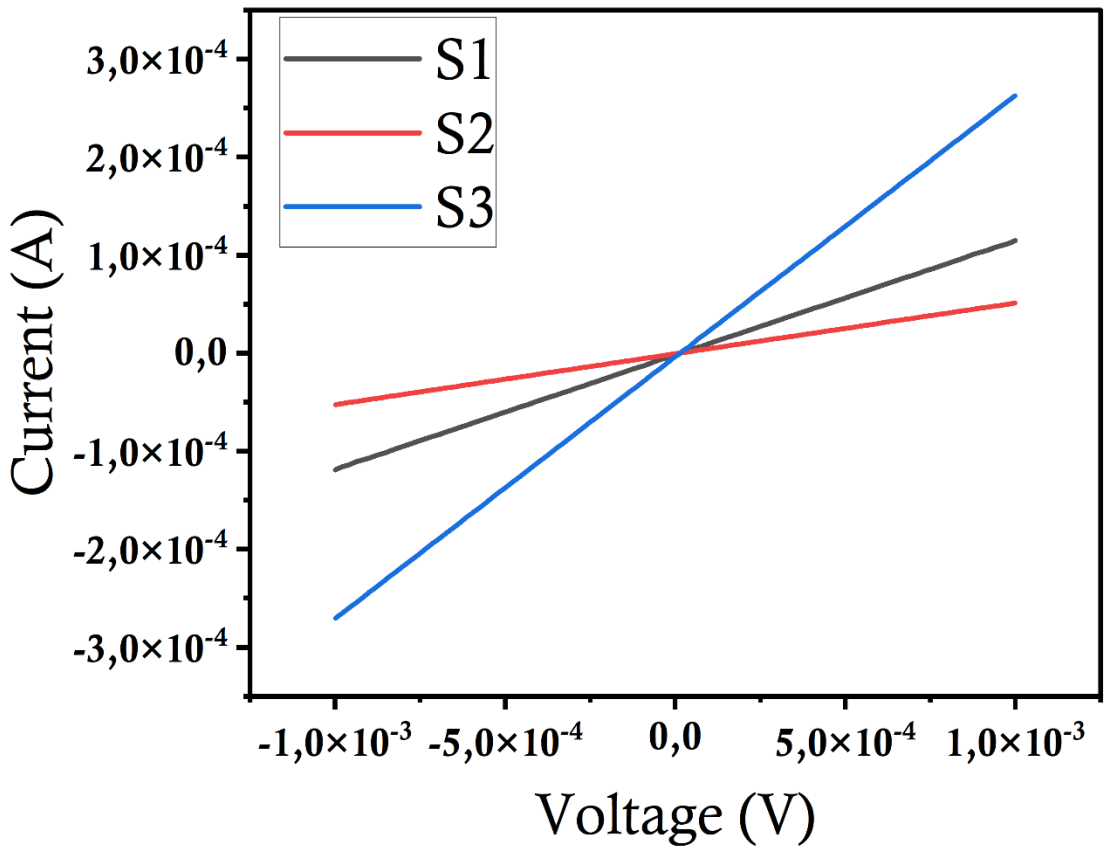

Figure B. The I-V characteristics of the developed TiO_2/CuO heterostructure-based sensors. Each line corresponds to different 3 samples (S1, S2, S3)

Statistical analisys

Table B. The average sensitivity of the different gas sensor devices at RT and 5 ppm

	S1	S2	S3
Ethanol	5.207	6.1	4.74
Acetone	4.8	5	2.45
N_2O	8.48	13.25	2
H_2	1.87	3.03	3.29
Toluene	2.62	3.14	3.11

We collected statistical data for 3 samples, where the sensitivity deviates depending on the sample. The hypothesis is to identify the statistical significance of the sensitivity dependence on the sample and gas type at the significance level of $p=0.05$.

Appendix – C

NAZARBAYEV UNIVERSITY
SCHOOL OF ENGINEERING AND DIGITAL SCIENCES

I-V characterization of p-n heterostructures obtained by GLAD

Madina Sarsembina, Amanzhol Turlybekuly , Almagul Mentbayeva, Zhumabay Bakenov

Department of Chemical and Materials Engineering, School of Engineering and Digital Sciences, Nazarbayev University

INTRODUCTION

In recent years, the development of gas monitoring devices/sensors are critical for environmental protection and for humans promptly. Due to their good characteristics as fast response, low cost, and small size gas sensors have become more prevalent in different fields from healthcare industries to food processing [1].

In breath sensing, metal oxide semiconductor (MOS) sensors are commonly utilized. MOS sensors are one of the finest alternatives for breath analysis because of its:

- compact size,
- ease of operation,
- low cost,
- and minimal maintenance [2].

However, conventional gas sensors with a single metal oxide layer, detect a shift in bulk resistance in response to gas contact, resulting in limited gas sensitivity and selectivity. For increasing gas sensitivity and selectivity, forming a p-n junction with MOS-based p-type and n-type electrodes is the best option

This research purpose to investigate gas sensor based on p-n junction heterostructures of MOS (TiO/CuO) with nanoscale architecture which is ultrasensitive for acetone and work at low temperature (room temperature)

EXPERIMENTAL PART

The p-n heterostructured (p-n HS) gas sensors were obtain by glancing angle deposition of metal target at reactive magnetron sputtering. The nanorods-like structures deposited in the sequentially or another words in same process.

The magnetron sputtering was carried out in the 20% oxygen/argon atmosphere. The width of the TiO_2 layer was ~ 120 nm, while the width of CuO layer was 30 nm. The smaller width of the CuO layer is derived by idea of matching of the depletion layer width with the CuO film one.

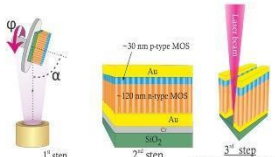

1st step The GLAD of sensing material

2nd step Top electrode deposition

3rd step Design of the sensor's micro architecture by the laser scribing

1 – bottom golden electrode
2 – p-n HN layer
3 – top electrode

Formation of gas sensor consists of general 3 steps: 1st The GLAD of p-n HS; 2nd deposition of top electrode; 3rd step – laser scribing for the increasing active surface area. According to the developed method more than 20 samples of p-n HS samples were obtained.

RESULTS AND DISCUSSION

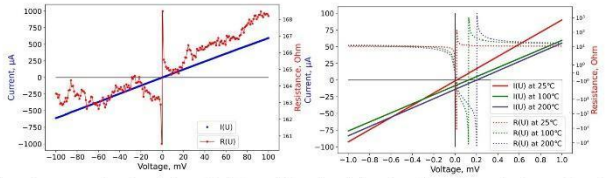

The dependence of current over the voltages belongs Ohmic Law and shows linear independence. Sharp changes of resistance at low voltages might indicate the electromotive force of the heterostructures between the layers p-n heterostructures. This electromotive force increases with the temperature

Dynamic gas response characteristics

Gas type	Response time, s	Recovery time, s
CO_2	~48 s	~40 s
Acetone	~51 s	~205 s
H_2	~33 s	~150 s

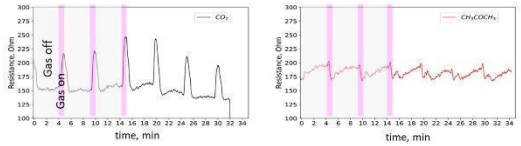

The measurements were conducted at RT and 10 ppm concentration of target gases was applied. The gas response was calculated by the equation 1.

$$N_{res}=|R_a-R_g|/R_a \times 100\% \quad (1)$$

The sensitivity test was conducted for reducing and oxidizing gases (CO2, H2, Acetone). The highest response was recorded for the CO2 gas ~ 60 %. The lowest response was observed for the acetone, ~10%. The fastest response time was recorded for the H2, highest recovery time observed for carbon dioxide.

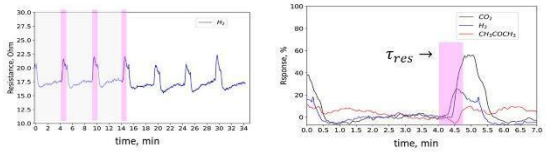

It is well known that the oxidizing CO_2 gas contributes holes after reacting with adsorbed oxygen, whereas the reducing H_2 gas catches holes after reacting with adsorbed oxygen, suggesting that the TiO_2/CuO HS n-type sensing capabilities. Despite the fact that the concentration of CO_2 gas is the same with H_2 gas, the current through the sensor is remarkably lowered by 10 times after CO_2 exposure. This suggests that under CO_2, the electron concentration in the n-TiO_2 NHs dramatically decreases.

CONCLUSION

The experimental results show possibility to develop RT gas sensors based on p-n nanointerfaces. The dynamic gas response parameters can be accepted as good. Despite good sensitivity and dynamic parameters the sensors don't show stable results. The further investigation to be continued to provide theoretical explanation of conductivity mechanisms at low potentials. The crystallographic characterization and phase verification problems should be solved.

REFERENCES

1. Ji, H., Zeng, W., & Li, Y. (2019). Gas sensing mechanisms of metal oxide semiconductors: a focus review. Nanoscale, 11(47), 22664-22684. https://doi.org/10.1039/c9nr07699a

2. Kwon, H., Yoon, J., Lee, Y., Kim, D., Baek, C., & Kim, J. (2018). An array of metal oxides nanoscale hetero p-n junctions toward designable and highly-selective gas sensors. Sensors And Actuators B: Chemical, 255, 1663-1670. https://doi.org/10.1016/j.snb.2017.08.173

Acknowledgments:

This research was supported by the research grant 021220CRP0122 "Development of highly sensitive MOS based nano-film gas sensors" from Nazarbayev University.

Presenter name : Madina Sarsembina
email : madina.sarsembina@nu.edu.kz

DATE :05/08/2022